Advances in Geo-Energy Research

Vol. 16, No. 2, p. 114-130, 2025

Original article

Development of a reactive transport solver in MATLAB Reservoir Simulation Toolbox using the fully-implicit sequential iterative approach

Sajjad Moslehi[1]*, Hossein Fazeli[2]*, Florian Doster[3], Shahin Kord[1]

[1]*Department of Petroleum Engineering, Petroleum University of Technology, Ahvaz PO Box 63187-14317, Iran*

[2]*School of Chemical, Petroleum, and Gas Engineering, Iran University of Science and Technology, Tehran PO Box 16765163, Iran*

[3]*Institute of GeoEnergy Engineering, Heriot-Watt University, Edinburgh EH14 4AS, UK*

Keywords:
Reactive transport modeling
MRST
sequential fully-implicit approach
fractured caprock

Cited as:
Moslehi, S., Fazeli, H., Doster, F., Kord, S. Development of a reactive transport solver in MATLAB Reservoir Simulation Toolbox using the fully-implicit sequential iterative approach. Advances in Geo-Energy Research, 2025, 16(2): 114-130.
https://doi.org/10.46690/ager.2025.05.04

Abstract:
Different operations dealing with the subsurface, such as subsurface CO_2 disposal, hazardous waste disposal, geothermal energy extraction, underground hydrogen storage, etc., can change the fluid/flow system underground. The injection of fluids with thermodynamic and chemical properties different from those of the reservoir fluid can trigger a series of chemical reactions, which may affect the fluid and/or rock properties. Depending on the system under study, these changes may be advantageous or unfavorable. Reactive transport modeling is a choice for investigating how these changes can alter the system. In this study, a reactive transport solver is developed in the MATLAB Reservoir Simulation Toolbox using the sequential fully-implicit approach. The developed reactive transport solver is illustrated using reactions and geometries using reactions and geometries relevant for assessing the sealing capacity of a fractured caprock of a deep saline aquifer used for underground CO_2 disposal, and the limitations and advantages of the approach are stated. Moreover, the results of the simulation for two fracture models, the discrete fracture matrix and embedded discrete fracture matrix models, are compared. The simulations demonstrate that hydrogen ion concentration or pH is the primary parameter affecting the extent of dissolution, while the other aqueous species concentrations are less influential. It is also shown that at higher flow rates, dissolution substantially occurs in the vicinity of the main fracture, along the flow direction, while at lower flow rates, because the injected fluid becomes fully buffered closer to the inlet, dissolution only occurs in the vicinity of the inlet over the course of the simulation. Applying the discrete fracture matrix and embedded discrete fracture matrix models to one of the scenarios demonstrates that both yield equivalent results.

1. Introduction

The topic of reactive transport in porous media has attracted enormous attention for investigating geochemical processes underground due to its role in understanding chemically-induced changes in subsurface reservoirs for CO_2 disposal (Fitts and Peters, 2013; Deng et al., 2015; Kampman et al., 2017), hazardous waste disposal (Gylling et al., 2016; Stein et al., 2017; Applegate and Appleyard, 2022), hydrogen storage (Hemme and Van Berk, 2018; Elgendy et al., 2023; Gholami, 2023), geothermal energy recovery (Pruess, 1991; Chen et al., 2018; de Hoop et al., 2021; Zhang et al., 2023), hydrocarbon production (Fan et al., 2010; Gong et al., 2014;

Yandy Scientific Press

*Corresponding author.
E-mail address: sajjadmoslehi127@gmail.com (S. Moslehi); HosseinFazeli@iust.ac.ir (H. Fazeli); F.Doster@hw.ac.uk (F. Doster); sh.kord@put.ac.ir (S. Kord).

Received October 22, 2024; revised January 5, 2025; accepted February 1, 2025; available online February 10, 2025.

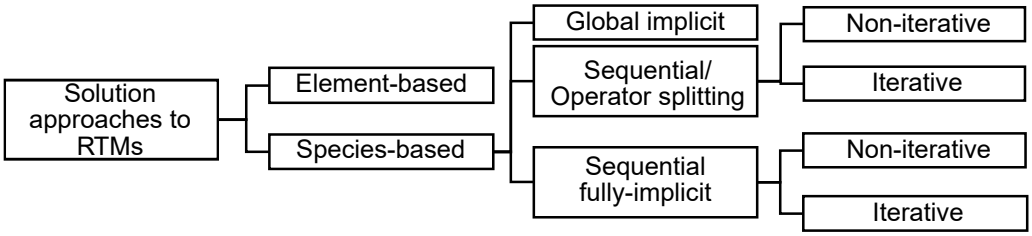

Fig. 1. Solution approaches to reactive transport problems.

Lee et al., 2017; Abd and Abushaikha, 2021), matrix acidizing (Liu et al., 1997, 2017; Shaik et al., 2018), and groundwater systems (Mayer et al., 2002; Molson et al., 2012). To investigate the effect of reactive transport for these applications, two approaches are usually used: Experiments and numerical modeling. In this study, the focus is on the numerical modeling of reactive transport in porous media. The solution schemes in numerical codes for reactive transport problems can be divided into two main categories: element-based and species-based schemes (Fig. 1).

There are few Reactive Transport Models (RTMs) coded with the element-based approach. The element-based formulation in reactive-transport modeling was first presented by Fan et al (2021) and is the formulation of Stanford's General Purpose Research Simulator (GPRS) (Cao, 2002; Jiang, 2007). Then, Colin et al. (2018) developed a reactive transport code in MATLAB Reservoir Simulation Toolbox (MRST) (Krogstad et al., 2015; Lie, 2019) using this formulation. In the element-based formulation, combination of the linearized equations transforms the species mass balances to element conservation equations. Chemical reactions enable elements to combine with other elements to form more complex compounds, though the elements that form the building blocks of the various compounds in the rock-fluid system are conserved. Thus, a mass balance equation can be written for each element, which may exist in any species and any phase (fluid or solid), such that the source terms due to reactions disappear (Fan et al., 2012).

The other main category of RTM solution approaches is the species-based approaches. In contrast to elements, species are not conserved but can appear and disappear through reactions. The species-based approaches themselves are divided into three categories: The global implicit approach (Hammond et al., 2005; Ahusborde et al., 2019; Seigneur et al., 2023), sequential (operator splitting) approach (Ahusborde et al., 2015; Ahusborde and El Ossmani, 2017), and the Sequential Fully-Implicit (SFI) approach. The sequential approaches themselves are broken down into two sub-categories: The Sequential Iterative Approach (SIA) and Sequential Non-Iterative Approach (SNIA) (Saaltink et al., 2001). In the SNIA approach, the mass transport and chemical reactions are decoupled and solved separately. This is referred to as operator splitting, where the transport equations are solved at each time step without the reaction relations and then followed by the reactive step. This approach introduces splitting errors that is usually reduced by solving the transport and reactive sub-problems iteratively, which is called the SIA approach. However, the SNIA and SIA require small time steps to be used, which could lead to slow convergence rates. This issue can be overcome by introducing the global implicit approach. The scheme is often accurate as both the transport and reaction steps are solved simultaneously with less restrictions on time step size, providing stability and robustness (Fahs et al., 2008). However, if the number of components in the system is large, this method suffers from an excessive computational time and memory requirements, especially in two and three-dimensional simulations (Abd and Abushaikha, 2021) because it requires the storage (large memory requirement) and inversion (long computational time) of a large linear system. In this study, the SFI approach is adopted to model reactive transport. This approach has already been used for non-reactive transport problems (Franc et al., 2023; Li et al., 2023) and coupled thermo-hydro-mechanical problems (Wang et al., 2024). SFI decomposes fully coupled non-linear (reactive) transport problems into non-linear sub-problems, and each sub-problem is solved fully implicitly. In this approach, dividing a global problem into a number of sub-problems requires the storage and inversion of several, but smaller Jacobian matrices, which reduces the overall computational time. Moreover, solving each sub-problem fully implicitly helps the approach be more numerically stable, i.e., this method can comparatively relieve the problems of numerical instability of the sequential methods and the high computational cost of the global implicit method (Franc et al., 2023).

Flow through fractured porous media is particularly sensitive to chemical reactions that lead to precipitation or dissolution. Fractures introduce new length and time-scales that require different modelling strategies for different purposes. These strategies are divided into two main categories depending on the representation of fractures: Implicit and explicit (Berre et al., 2019). For large scale investigations the implicit approach is the method of choice, but it requires a robust understanding of the processes in order to be able to represent them accurately (if at all possible) through upscaled models. This is generally not the case for reactive processes and hence for RTM, a model with an explicit representation of fractures is more appropriate to improve our understanding of the coupling. Thanks to the explicit representation of fractures, complex connectivity, geometry, and heterogeneity of fractures are accounted for. There are already several reactive transport models coded using the discrete fracture models (Table 1).

In the MRST (Krogstad et al., 2015; Lie, 2019) however, a module for species-based reactive transport modelling is lacking. In this study, the Discrete Fracture Matrix (DFM)

Table 1. RTMs using discrete fracture models.

Reference	Fracture model	Reactions	Field of study
Machado et al. (2023)	EDFM	Calcite, quartz, kaolinite, K-feldspar, albite, dawsonite, and halite dissolution/precipitation	CO_2 disposal in carbonate reservoirs
de Hoop et al. (2020)	DFM	Carbonate dissolution/precipitation	Geothermal reservoirs
Song et al. (2022a)	DFM	Silica dissolution/precipitation	Geothermal reservoirs
Song et al. (2022b)	DFM	Silica dissolution/precipitation	Geothermal reservoirs
Zhang et al. (2023)	EDFM	Silica dissolution/precipitation	Geothermal reservoirs
Banshoya et al. (2023)	DFM	Calcite and anhydrite dissolution/precipitation	Non-isothermal
Vu et al. (2019a))	DFM	Tetrachloroethylene (PCE) degradation	Hazardous waste disposal
Applegate and Appleyard (2022)	DFM	Calcite dissolution/precipitation	Hazardous waste disposal
Gylling et al. (2016)	DFM	Sorption of cesium onto biotite of rock grains	Hazardous waste disposal
Stein et al. (2017)	DFM	Reactive radionuclide transport	Hazardous waste disposal
Vu et al. (2019b)	DFM	PCE and trichloroethylene degradation	Hazardous waste disposal
Gong et al. (2014)	DFM	Methane sorption/ desorption	Coalbed methane reservoirs
Yan et al. (2018)	DFM	Gas adsorption/desorption	Gas storage in shale gas reservoirs
Jiang et al. (2022)	DFM	Calcite dissolution	Karst genesis in carbonate aquifers
Jiang et al. (2023)	DFM	Calcite dissolution	Karst genesis and wormhole formation in carbonate aquifers
Li et al. (2020)	EDFM	Gypsum and limestone dissolution/precipitation	Hypogene speleogenesis in aquifers
Liu et al. (2017)	DFM	Carbonate mineral dissolution	Matrix acidizing operation and wormhole formation in carbonate reservoirs
Sherman et al. (2023)	DFM	Kinetic reaction (A + B $\rightarrow$ C)	Interaction of 2 solute plumes
Andrews et al. (2023)	DFM	Albite dissolution	Hillslope weathering
Molson et al. (2012)	DFM	Calcite, siderite, gibssite, gypsum, ferrihydrite, and quartz dissolution/precipitation	Acid mine drainage

(Karimi-Fard et al., 2004) and Embedded Discrete Fracture Matrix (EDFM) (Moinfar et al., 2014) modules are expanded for species-based reactive transport. The DFM and EDFM fracture models are used because both are easily accessible in MRST. The resulting module builds on a fully-implicit sequential approach to model coupled fluid flow, solute transport, and chemical reactions in both fractured or non-fractured porous media. This code is capable of modeling aqueous reactions as equilibrium reactions and various kinetically-controlled single-mineral or multi-mineral dissolution/precipitation reactions.

The applicability of the solver is illustrated for different reactive transport problems and assess its advantages and drawbacks with the help of parameters and geometries for a fractured caprock, the Eau Claire formation. The Eau Claire formation overlies the Mt. Simon aquifer which is used as a reservoir for CO_2 disposal in the Illinois Basin. This caprock is mainly made of dolomite (Barnes et al., 2009; Palkovic, 2015; Gilmore et al., 2016) and in this study is considered as a fractured caprock because dolostone is prone to having fractures due to its high brittleness even at high confining

pressures (Billings, 1972).

2. Modelling assumptions and mathematical equations

2.1 Modelling assumptions

The reactive transport solver is developed based on the following modelling assumptions:

- The pore-space is completely filled by a liquid phase that is incompressible and whose composition does not alter the viscosity.
- The pressure equation is derived from the mass conservation (continuity) equation of the dominant species in the desired phase, i.e., among the chemical species, it is assumed there exists one dominant species and that the minor species have no significant influence on the mass balance equations of the dominant species, i.e., the minor species do not significantly alter density and viscosity.
- Flow in the porous medium and the fractures is controlled by Darcy's law.
- The system is isothermal and heat production or consumption by reactions is neglected.
- The matrix of the porous medium is made of a single mineral.

2.2 Governing equations

With the modelling assumptions, the system is described by a set of governing equations consisting of the pressure equation, mass transport equations, and reaction relations. For n primary species, and N chemical reactions, one pressure equation, n mass transport equations, and N reaction relations are solved for each grid block, which equals a total number of $1+n+N$ equations.

2.2.1 Pressure equation

As stated in Section 2.1, the pressure equation is derived from the mass conservation equation of the dominant species of the desired phase, which is liquid water in this study. The typical application for this approach is dilute water solutions. The pressure equation then reads as:

$$-\nabla\cdot(\boldsymbol{u_w})+q_w^W=\frac{\partial\phi}{\partial t} \tag{1}$$

where $\boldsymbol{u_w}$ is the Darcy velocity of water, q_w^W is the water well (sink/source) term, ϕ is rock porosity, and t is time. The Darcy velocity is given by:

$$\boldsymbol{u_w}=-\frac{\boldsymbol{K}}{\mu_w}(\nabla P_w-\rho_w\boldsymbol{g}) \tag{2}$$

where $\boldsymbol{K}$, μ_w, P_w, ρ_w, and $\boldsymbol{g}$ are permeability tensor, water viscosity, water pressure, water density, and gravitational acceleration vector, respectively.

These equations are discretized using a finite volume approach with a two-point flux approximation. Because of the modular structure of MRST, the reactive transport solver is flow discretization independent. This is illustrated later with the help of a DFM and an EDFM approach. Details for the discretization for the porous matrix are provided in (Lie, 2019) while the details for the fractures of the DFM and EDFM approach are given in chapters 9 and 11 of (Lie and Møyner, 2021), respectively.

2.2.2 Mass transport equations

To write the mass transport equations, the set of all the chemical species are split into primary and secondary species. Each reaction expresses the formation of a secondary species from the set of primary species, also called basis species or components (Morel and Hering, 1993). Primary species are a set of linearly independent chemical entities such that every secondary species can be uniquely represented as a combination of those primary species, and no primary species can be represented by other species other than itself (Yeh and Tripathi, 1989). The mass transport equation is the mass conservation (continuity) equation of primary species and their corresponding secondary species based on reactions. The mass conservation equation for the primary species i and its corresponding secondary species $j=1-n_j$ based on the network of reactions is:

$$\begin{aligned}&-\nabla\cdot\left(\left[C_i+\sum_{j=1}^{n_j}a_jC_j\right]\boldsymbol{u_w}-\phi D_{ij}\nabla\left[C_i+\sum_{j=1}^{n_j}a_jC_j\right]\right)\\&+q_{ij}^W=\frac{\partial\left(\phi\left[C_i+\sum_{j=1}^{n_j}a_jC_j\right]\right)}{\partial t}\end{aligned} \tag{3}$$

where C_i is the concentration of the primary species i, n_j is the total number of secondary species, and a_j is the coefficient of the concentration of the secondary species j (C_j) based on the special form of the stoichiometric matrix, described by Ahusborde et al. (2015). D_{ij} is the diffusion/dispersion tensor of primary and secondary species, and q_{ij}^W is the well (source/sink) term of primary and secondary species. The term using the divergence operator represents the flux term of the species, which includes both the advective and diffusive fluxes and the right-hand side of the equation is the accumulation term of the primary and secondary species.

2.2.3 Reaction relations

In reactive transport modeling, reactions are divided into two categories: Equilibrium and kinetic reactions. By conventions, equilibrium reactions are defined as chemical reactions that are sufficiently fast and reversible, and kinetic reactions as those that are slow or irreversible. In other words, chemical reactions can be categorized into kinetic reactions and equilibrium reactions based on their rates. In reactive transport modelling, if the time scale of reaction is shorter than the time scale of transport, the reaction is considered to be at local equilibrium and if the time scale of reaction is longer than the time scale of transport, the reaction is said to be kinetically controlled. In the developed module, all the aqueous reactions are treated as equilibrium reactions and all mineral reactions as kinetic reactions.

Equilibrium reactions are represented by algebraic equations. In equilibrium reactions, because the reactants and products reach the state of chemical equilibrium quickly, a thermodynamic approach is normally taken to characterize these reactions. The general mass action law (mass action

equation) is written as:

$$K^{eq} = Q \tag{4}$$

where K^{eq} is the equilibrium constant that may depend on temperature or pressure and Q is called the reaction quotient, which is the product of species concentrations or activities powered by their corresponding stoichiometric coefficients that have a minus sign for reactants.

Kinetic reactions are represented by ordinary differential equations. The reaction relation corresponding to a kinetic reaction is essentially the mass conservation equation for the mineral in that reaction. The kinetic relation for a mineral is as follows:

$$r = \frac{\mathrm{d}C_m}{\mathrm{d}t} \tag{5}$$

where C_m is the concentration of the mineral, and r is the rate of the kinetic reaction., The Transition State Theory (TST) rate equation is used for the calculation of the rate of the desired kinetic reaction, which is expressed as (Lasaga, 1984; Steefel and Lasaga, 1994; Nghiem et al., 2004):

$$r = kA_m\left(1 - \frac{\Pi_i C_s^{\vartheta_s}}{K^{eq}}\right) \tag{6}$$

where r is the is the rate of the dissolution/precipitation reaction (positive values indicate dissolution, and negative values precipitation), k is the rate constant (moles per unit mineral surface area and unit time), A_m is the mineral specific reactive surface area, C_s is the concentration of the fluid species s, ϑ_s is the stoichiometric coefficient of the species s with a minus sign for reactants.

2.3 Auxiliary equations

2.3.1 Rock porosity relations

The change of the rock pore volume with pressure and rock dissolution/precipitation is considered using the following equations (Nghiem et al., 2004), respectively:

$$\phi = \phi_0 \exp\left[c_r\left(P - P_0\right)\right] \tag{7}$$

$$\phi = \phi_0 + N_{m\ 0} V_{m,mineral} - N_m V_{m,mineral} \tag{8}$$

where $N_{m\ 0}$ and N_m are the mineral moles at the reference (initial) time step and the desired time step, respectively, $V_{m,mineral}$ is the mineral molar volume, and c_r is the rock compressibility.

2.3.2 Porosity-permeability relations for rock matrix and fractures

The change in rock permeability for the rock matrix due to porosity change is modelled using the Kozeny-Carman relation (Bear, 2013):

$$\frac{K}{K_0} = \left(\frac{\phi}{\phi_0}\right)^3 \left(\frac{1-\phi_0}{1-\phi}\right)^2 \tag{9}$$

For intrinsic fracture permeability calculation, fractures are assumed to follow the cubic law. Therefore, intrinsic fracture permeability is calculated by:

$$K_f = \frac{a^2}{12} \tag{10}$$

where a is the hydraulic fracture aperture. According to Darcy's law, volumetric flow rate in a fracture is proportional to the product of fracture permeability and the cross-sectional area of the fracture. The former is proportional to the square of the fracture aperture and the latter is proportional to the fracture aperture. As such, the volumetric flow rate is proportional to a^3. As a result of this relationship, Eq. (10) is often called the cubic law.

Fracture permeability changes can be approximated using the porosity change and an assumption of plane parallel fractures of uniform aperture. The modified permeability is then given by (Xu et al., 2004):

$$\frac{K}{K_0} = \left(\frac{\phi}{\phi_0}\right)^3 \tag{11}$$

2.3.3 Reactive surface area relation

The following relation is used to update the reactive surface area with change in the moles of minerals through dissolution or precipitation (Nghiem et al., 2004):

$$A_m = A_{m\ 0} \cdot \frac{N_m}{N_{m\ 0}} \tag{12}$$

where $A_{m\ 0}$ and A_m are the reactive surface area of mineral at time 0 and the desired time, respectively.

3. Solution approach

A finite-volume discretization on an unstructured triangular mesh (for DFM) and Cartesian mesh (for EDFM) is applied. Accumulation terms are discretized with backward Euler approximation.

To solve the set of governing equations, the parameters of the next time step are used (fully-implicit) and the problem is divided into three sub-problems that are solved sequentially (sequential approach) (Xu and Pruess, 2001; Fang et al., 2003; Hammond et al., 2007; Ahusborde and El Ossmani, 2017), known as the SFI approach. The Newton-Raphson method is used for each subproblem in this code to solve the system of highly non-linear mathematical equations. To use the Newton-Raphson method, the Jacobian matrix needs to be constructed, which requires the differentiation of residual equations with respect to different independent variables. Here, the underlying automatic differentiation framework of MRST is exploited to construct Jacobian matrices. Combining this technique with discrete averaging and differential operators enables us to write very compact simulator codes in which the models are implemented almost in the same form as they are written in the underlying mathematical equations (Lie, 2019). The first sub-problem is devoted to calculating pressure (i.e., fluid velocity) in porous media using the pressure equation. In this first sub-problem, by obtaining fluid pressure, pore volume can be updated. The second sub-problem consists of mass transport equations of primary species and their corresponding secondary species, and the third sub-problem consists of the relations of equilibrium and kinetic reactions. The third sub-

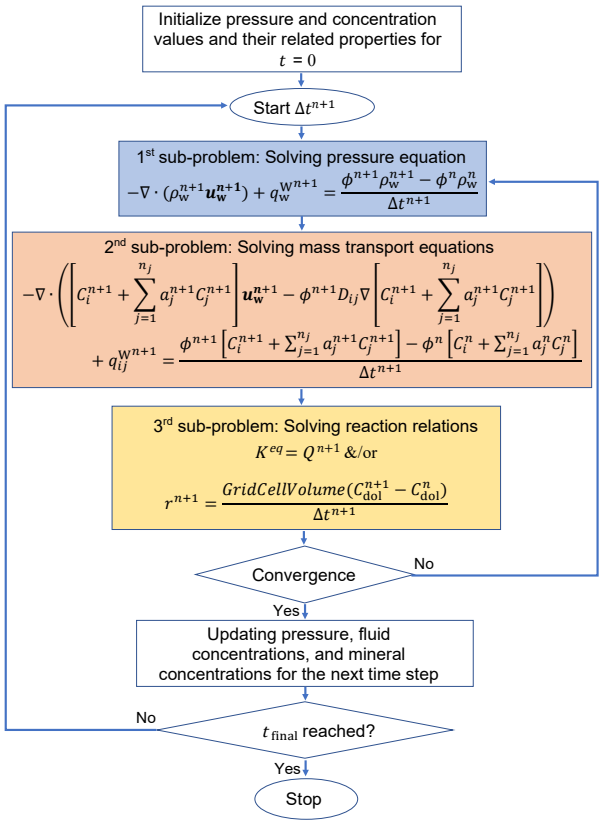

Fig. 2. Flowchart of the developed reactive transport code.

problem, which represents the reactive part, updates the concentrations of mineral or minerals in the system. By having the mineral concentration, properties such as pore volume (i.e., porosity), permeability, and reactive surface area of the mineral can be updated. After solving all the three sub-problems, another convergence check is implemented, which ensures that the summation of all the three norms of residuals calculated in each sub-problem is lower than a certain tolerance. The flowchart of the reactive transport code is shown in Fig. 2.

4. Reactive transport code verification

For validating the reactive code, the results from our module for a one-dimensional reactive transport problem without fractures are compared with the results of the geochemical compositional simulator from CMG, GEM-GHG (Nghiem et al., 2004; Nghiemw et al., 2004). Dolomite dissolution in a one-dimensional horizontal reservoir extending 1.37 m (this length is chosen for the reason mentioned in Section 5.1) in the x direction with 200 grid cells and 0.1 m in both the y and z directions is considered. The rock and fluid properties, and all the geochemical properties are given in Table 2. The initial pressure of the system is 2,400 psia. The water is injected into the left-most grid block with a constant flow rate of 10^{-4} m^3/day (Neumann BC) and produced from the rightmost grid block under a constant bottom-hole pressure of 2,400 psia (Dirichlet BC). The total simulation time is 4 days.

The simulations are done with non-iterative and iterative SFI approaches, and the concentration profiles of the chemical species are plotted in Figs. 3 and 4. The red symbols represent the results from our MRST module and the blue lines represent the results from GEM-GHG. The figures show that the results of the iterative SFI match well with the CMG results, but the non-iterative SFI has not given correct concentration profiles, which indicates that in this reactive transport problem, there is strong coupling between the mass transport and the reaction sub-problems.

Table 2. Model grid, rock, and fluid properties (Barnes et al., 2009; Salih and Dastgheib, 2017; Mehnert et al., 2019).

Type	Property		Value
Grid	Total length (m)	x-direction	$1.27 + 0.10$
		y-direction	0.60
		z-direction	1
	Number of cells in EDFM model	x-direction	137
		y-direction	60
		z-direction	1
Rock	Matrix porosity (%)		5.9
	Matrix permeability (m^2)		5.9215×10^{18}
	Matrix compressibility (1/Pa)		7.2519×10^{-10}
	Fracture aperture (mm)		0.01
Fluid	Phase type		Single phase of water
	Viscosity (Pa·s)		10^{-3}

5. Problem setup

5.1 Model domain, rock, and fluid properties

The computational domain is shown in Fig. 5. The domain consists of 2 parts. A fractured region considered as a section of a fractured rock previously modelled by several researchers (the small pictures in Fig. 5) (Hu and Rutqvist, 2022; Steefel and Hu, 2022), and a non-fractured slab of rock (approximately 10 cm wide) that is added at the left boundary to reduce boundary effects with the fractures. The domain is two dimensional and discretized using Cartesian mesh (8,600 matrix and fracture cells) and triangular mesh (6,729 matrix and fracture cells). For generating the triangular mesh, an open-source two-dimensional quality mesh generator and Delaunay triangulator named Triangle program (version 1.6) is used (Shewchuk, 1996). Because the computational domain is two dimensional, in DFM and EDFM models, the modelled fractures are one dimensional, which are represented as lines with desired widths.

The information of the geometry, rock, and fluid is given in the table below. Rock permeability of the rock is assumed to be isotropic.

For mass transport equations, the diffusion coefficients of all the chemical species are set to 10^{-9} m^2/s (Deng et al., 2015).

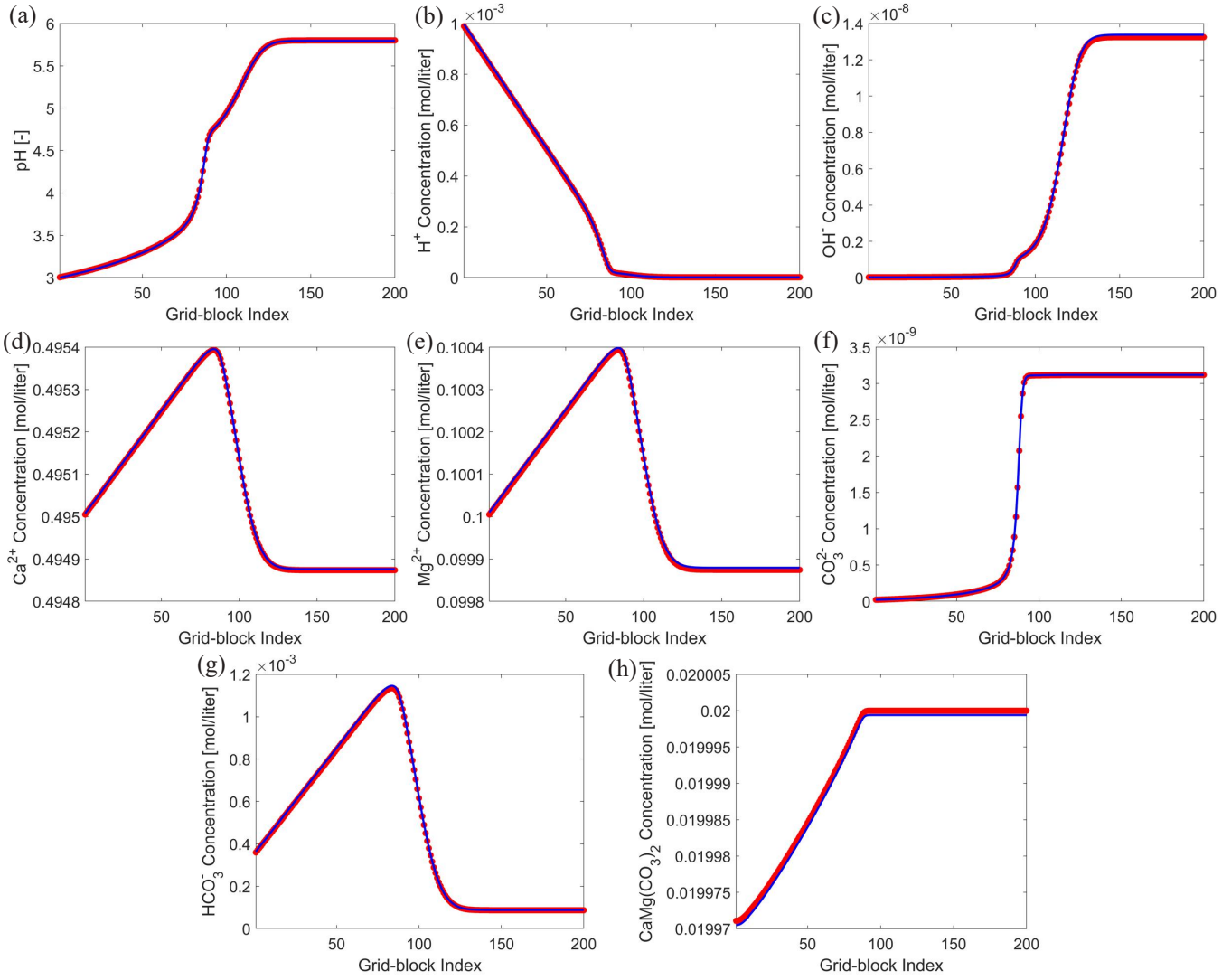

Fig. 3. Comparison of chemical species profiles from the iterative SFI approach in MRST and GEM-GHG for 1-D case at the end of simulation time. Red symbols represent MRST results using iterative SFI, and blue lines represent GEM-GHG results. (a) pH, (b) H^+, (c) OH^-, (d) Ca^{2+}, (e) Mg^{2+}, (f) $CO_3{}^{2-}$, (g) $HCO_3{}^-$ and (h) $CaMg(CO_3)_2$.

5.2 Model geochemistry

In this problem, H^+, OH^-, H_2O, Ca^{2+}, Mg^{2+}, $CO_3{}^{2-}$, HCO^{3-}, $CaMg(CO_3)_{2(s)}$ are the chemical species. The set of primary species in the system is H^+, H_2O, Ca^{2+}, Mg^{2+}, and $HCO_3{}^-$. The initial chemical composition of the formation brine (Table 3) is based on the fluid chemistry of the Mt. Simon brine collected from a well in the Vermillion County (Keller, 1983; Labotka et al., 2015). Four different injected water compositions are considered to show their effect on dissolution/precipitation reactions occurring in the porous medium. The injected water composition 1 is the most realistic composition chosen for CO_2 disposal in deep saline aquifers. The injected water composition 2 is different from 1 in terms of the concentrations of all ions except hydrogen ion to investigate the effect of the changes on the system. The only difference between the injected water composition 3 and 1 is that the 3rd one is less acidic, which assesses the effect of pH change on the system, and the injected water composition 4 is chosen such that precipitation occurs in the system. Note that for rapid changes in fluid or mineral concentrations in the system time-step constraints become prohibitive and convergence is not achieved.

For determining the initial composition of the formation water and the composition of the injected water, all the chemical reactions are assumed as equilibrium reactions. To this end, a reactive transport solver developed by McNeece et al. is used (Colin et al., 2018). For the dissolution and precipitation scenarios, the initial dolomite content of the rock is 0.020 and 1.326×10^{-4} mol per liter, respectively. Note that the fluid species concentrations are defined over the net fluid (= pore) volume and the solid concentration is defined over the entire control volume which includes fluids and solids.

The information of the chemical reactions involved in the dissolution/precipitation of dolomite is given in Table 4. The common practice in groundwater modeling is adopted by treating all of the intra-aqueous reactions (homogeneous or

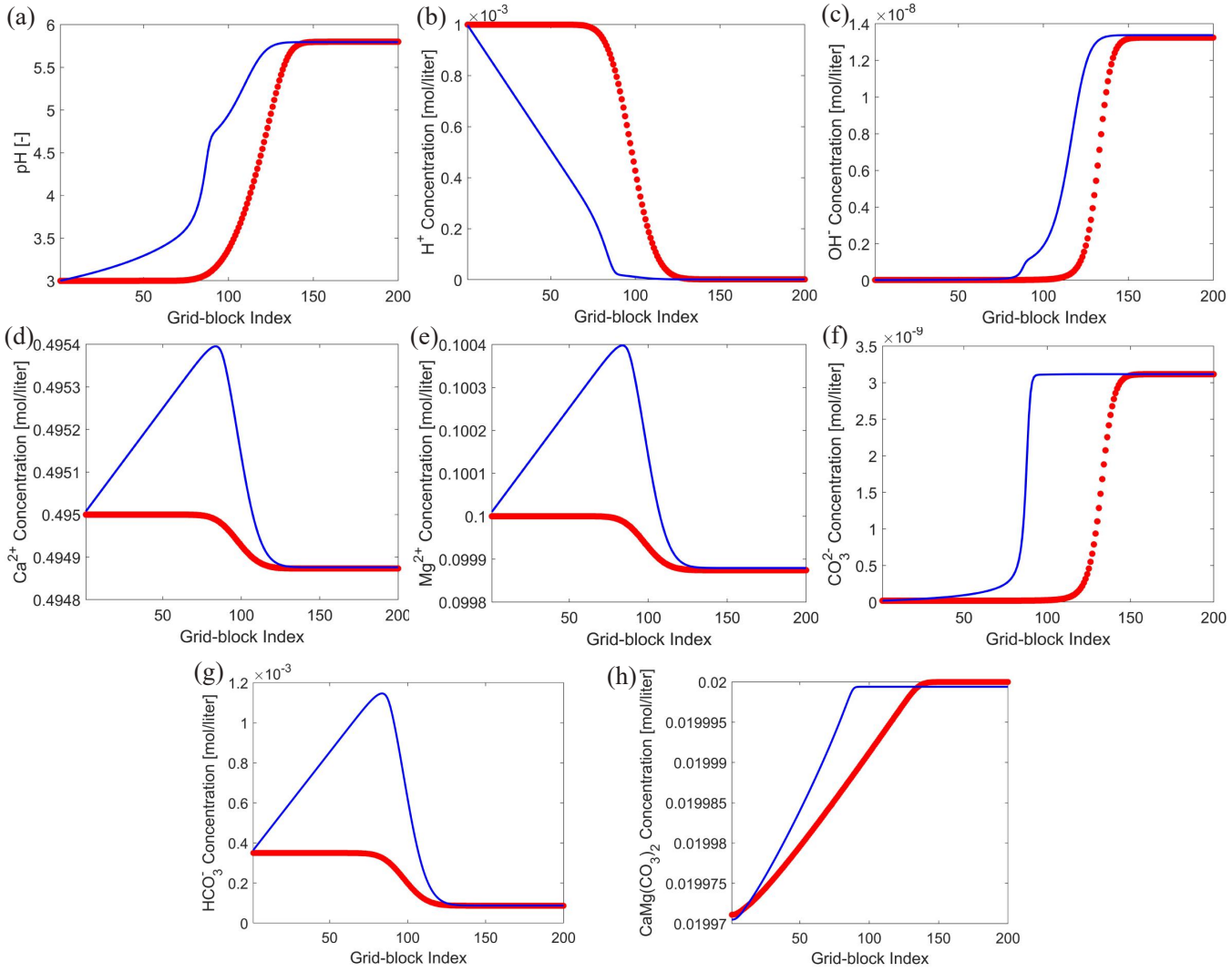

Fig. 4. Comparison of chemical species profiles from the non-iterative SFI approach in MRST and GEM-GHG for 1-D case at the end of simulation time. Red symbols represent MRST results using non-iterative SFI approach, and blue lines represent GEM-GHG results. (a) pH, (b) H^+, (c) OH^-, (d) Ca^{2+}, (e) Mg^{2+}, (f) $CO_3{}^{2-}$, (g) $HCO_3{}^-$ and (h) $CaMg(CO_3)_2$.

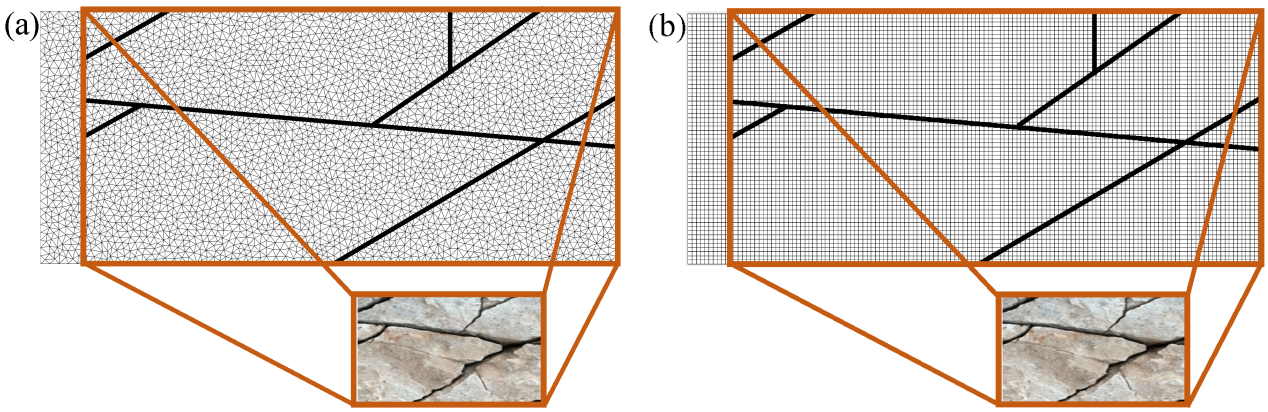

Fig. 5. Computational domain and the picture of a fractured rock (Steefel and Hu, 2022). (a) DFM and (b) EDFM.

Table 3. Injected water and initial formation brine composition (Keller, 1983; Labotka et al., 2015; Salih and Dastgheib, 2017).

Component concentration (molar)	Formation water	Injected water			
		Composition 1 (dissolution)	Composition 2 (dissolution)	Composition 3 (dissolution)	Composition 4 (precipitation)
$[Ca^{2+}]$	0.495	0.495	10^{-5}	0.495	0.095
$[Mg^{2+}]$	0.1	0.1	10^{-5}	0.1	0.005
$[HCO_3^-]$	8.7×10^{-5}	3.5×10^{-4}	10^{-5}	3.5×10^{-4}	5.443×10^{-4}
$[H^+]$	$10^{-5.8}$	10^{-3}	10^{-3}	10^{-4}	10^{-6}

Table 4. Reaction properties (Parkhurst and Appelo, 1999; Palandri and , 2004; Thibeau et al., 2007; Fan et al., 2012).

Equation	Type	$\log K^{eq}$		$\log K$		ΔH (J/mol)	E_a (J/mol)	$A_{m\ 0}$ (m^2/m^3)
		25 °C	35 °C	25 °C	35 °C			
$H_2O \leftrightarrow H^+ + OH^-$	Equilibrium	-13.9951	-13.6778	/	/	55,814.6	/	/
$CO_3^{2-} + H^+ \leftrightarrow HCO_3^-$	Equilibrium	10.3288	10.2455	/	/	-14,698.4	/	/
$CaMg(CO_3)_2(s) + 2H^+ \leftrightarrow 2HCO_3^- + Ca^{2+} + Mg^{2+}$	Kinetic	2.5135	2.1726	-9.22	-9.022	-59,965.1	34,800	88

Table 5. Scenarios information.

Dissolution/ Precipitation	Scenario	Simulation time (days)	Injected water composition number	Injection rate ($10^{-5}m^3$/day)
Dissolution	Diss1	50	1	32
	Diss2	50	1	160
	Diss3	50	1	320
	Diss4	7	2	160
	Diss5	7	3	160
Precipitation	Prec1	10	4	3,200

aqueous reactions) as equilibrium and all others as kinetic reactions (heterogeneous or mineral reactions). The reaction equilibrium constants are recalculated at the caprock temperature using the van't Hoff equation and the rate constant of the dolomite kinetic reaction is recalculated using the Arrhenius equation. The caprock temperature is considered as the temperature at the centroid of the caprock 1,050 meters deep, which is equal to 35 °C based on the temperature log reported in 2012 (Mehnert et al., 2019).

Mineral molar volume ($V_{m,mineral}$) of dolomite is 3.36×10^{-5} $m^3 \cdot mol^{-1}$ (Luhmann et al., 2014).

5.3 Initial and boundary conditions

The initial pressure of the system is set equal to 2,400 psia (Barnes et al., 2009). The water is injected through the leftmost grid blocks with a constant flow rate (the list of flow rates is specified in Table 5) (Neumann BC) and all the rightmost grid blocks of the computational domain are under a constant pressure of 2,400 psia (Dirichlet BC). The upper and lower boundaries are set to have no-flow boundary conditions. Numerical dispersion is minimized by constraining the time steps to maintain the Courant-Friedrichs-Lewy (CFL) condition (Pruess et al., 2002) for advective flow.

6. Discussion of illustrative scenarios

Numerical simulations are conducted to model caprock-brine interactions in the caprock formation. Due to rapid changes at the beginning of the simulation, selecting time step sizes in an ascending order greatly solves convergence issues. At the beginning, small time step sizes are needed, but after some time the changes become smoother (in our studies), and so the solution converges with larger time step sizes.

The scenarios are specified in Table 5. Simulations are done at different injection flow rates (transport rates) to assess the effect of the ratio of reaction rate to transport rate (typically quantified with the Damkohler number) on the system. Furthermore, different injected water compositions are considered to show their effect on chemical changes occurring in the porous medium (Table 3), but the composition number 1 is the most realistic composition chosen for CO_2 disposal in deep saline aquifers. Therefore, this composition is used as a base case for investigating the effect of injection rate.

At the end, the results of DFM and EDFM models for Diss1 are compared.

6.1 Injection (leakage) rate effect

The effect of injection (leakage) rate is examined by conducting the simulation at three different injection (leakage) rates: 32×10^{-5} (Diss1), 160×10^{-5} (Diss2), and 320×10^{-5}

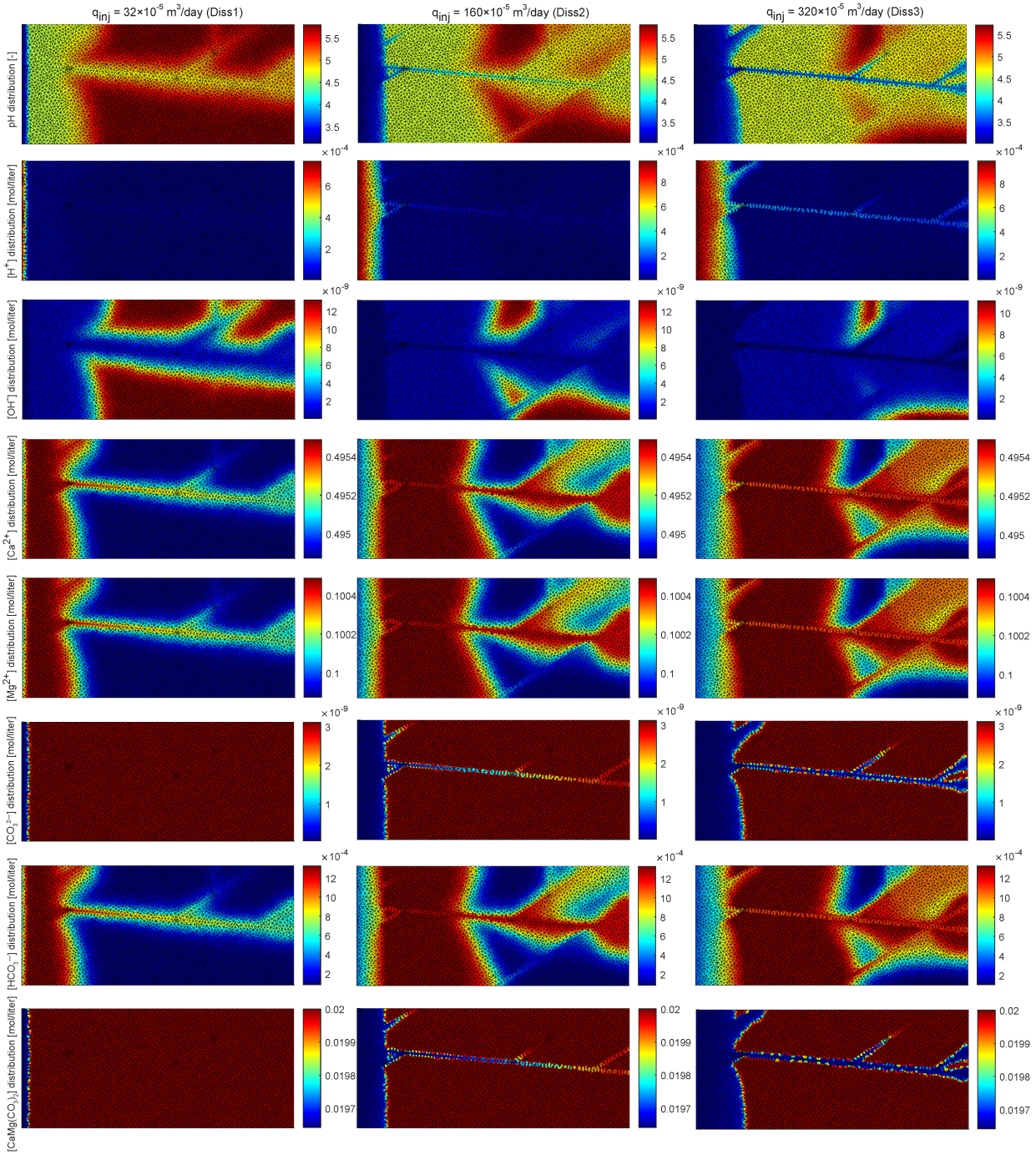

Fig. 6. Distribution of aqueous and mineral species concentrations after 50 days of injection at different injection rates (Diss1, Diss2 and Diss3).

(Diss3) m^3/day. Fig. 6 shows the distribution of the chemical species concentrations in the model after 50 days of injection. At 32×10^{-5} m^3/day, dissolution has occurred only in the vicinity of the inlet during the simulation time. When the injection rate is higher, the injected acidic water can move downstream by a larger distance before becoming fully buffered, so it can dissolve a larger area of the dolomitic rock.

Dissolution patterns of dolomite at the same injected volume are plotted in Fig. 7. As shown, when the injection rate is low (Diss1), i.e., when the flow rate is lower, dissolution mostly occurs in the vicinity of the inlet. On the other hand, when the injection rate is higher (Diss2 and Diss3), the injected water has not only dissolved near the inlet, but also influenced the fractures and their surrounding grid blocks, and even in Diss3, dolomite near the outlet is also dissolved. These results are also experimentally observed by several researchers (Luhmann et al., 2014; Deng et al., 2015) and suggest that low flow rates can cause extensive dissolution at the inlet of a flow system, while high flow rates can produce uniform dissolution patterns along the length of the flow path, where fluid moves

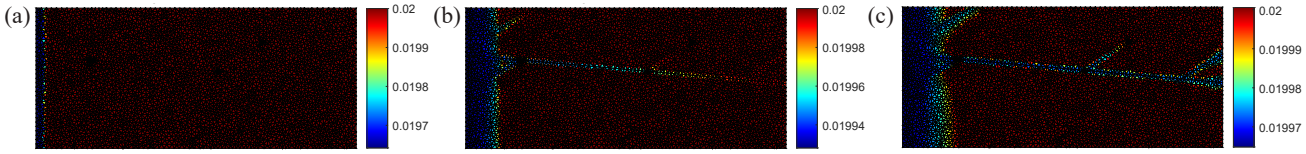

Fig. 7. Dolomite concentration [mol/liter] patterns at the same injected volume (0.016 $m^3 \equiv 0.33$ pore volume) for different injection rate. (a) Diss1, (b) Diss2 and (c) Diss3.

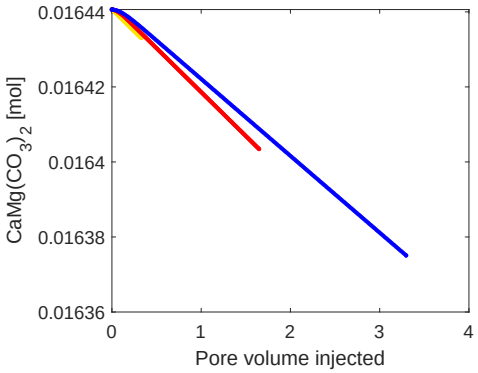

Fig. 8. Total dolomite mole change over pore volume injected, yellow markers: Diss1, red markers: Diss2 and blue markers: Diss3.

through the system before it is fully buffered. Although dissolution is more extensive in high injection rates, minimum dolomite concentration is larger than the case in which injection rate is low. Based on Fig. 7, in the case of low injection rate (Diss1) the minimum dolomite concentration is about 0.0197 mol/liter while at the high injection rate (Diss3), the minimum dolomite concentration is about 0.01997, which is larger than the low injection rate. Therefore, as the flow rate is higher, minimum dolomite concentration is larger. Fig. 8 shows that as the injection rate is higher, less dissolution occurs in the porous medium after equal pore volume injected.

The evolution of effluent concentrations of different aqueous species versus pore volume injected for Diss1, Diss2, and Diss3 are plotted in Fig. 9. Based on the graphs, the changes occurring in Diss3, in which the flow rate is high, are much more than Diss1. The changes in the slope of effluent concentrations of the chemical species at high injection rates are believed to be because of the spatial heterogeneity of the porous medium (the presence of fractures). The effluent carbonate concentration for Diss3 shows a small concentration rise after about 5 days of injection (0.25 PVI). This slight increase is because as rock dissolves, bicarbonate concentration increases. Based on the second reaction in Table 4, as the bicarbonate concentration increases, due to the Le Chatelier's Principle the position of equilibrium shifts to counteract the change to reestablish an equilibrium. As a result, some carbonate is produced, which results in its concentration rise.

6.2 Injected water composition effect

Scenarios Diss1 to Diss3 are all simulated using the same injected water composition. As an example, concentration distributions of aqueous species and dolomite for the scenario with the highest injection rate (Diss3) after 50 days of injection are depicted in Fig. 10. As shown, as the water is injected into the domain, hydrogen ion concentration increases due to the higher acidity of the injected water. The pH reduction in the reservoir triggers dolomite dissolution, which leads to calcium and magnesium release but due to the lower calcium and magnesium concentrations in the injected water, as more water is injected, their concentrations decrease near the inlet. Furthermore, the dissolution of dolomite yields bicarbonate. Fig. 10 shows this bicarbonate concentration increase where dissolution is occurring. However, similar to calcium and magnesium concentration patterns, as more water is injected, the lower bicarbonate content of the injected water reduces the bicarbonate concentration of the pore water, which is shown in the upstream direction of the flow. Based on the second chemical reaction in Table 4, as the bicarbonate concentration increases, more carbonate is produced, but due to the very large equilibrium constant of this reaction, small amount of carbonate is produced. The very small carbonate production and the low content of carbonate in the injected water ultimately leads to overall carbonate concentration reduction and no carbonate concentration increase is explicitly observed (later by investigating the effluent carbonate concentration over time, it can be seen that carbonate concentration slightly increases, shown in Fig. 9).

Porosity distribution in Diss3 after 50 days of injection is also shown in Fig. 10. Porosity changes due to dissolution/-precipitation of dolomite. Also, pore pressure has an impact on porosity. However, because the extent of porosity change due to dissolution is much larger than due to pressure, the pressure pattern is not reflected in the porosity distribution.

The concentration distribution of aqueous and mineral species for Diss4 are shown in Fig. 11. This composition of injected water also leads to dissolution, but the concentration patterns of the aqueous species are different from other dissolution scenarios. Fig. 12 shows a comparison of dolomite concentrations for different injected water compositions after 7 days of injection. It can be seen that although the concentrations of the chemical species except hydrogen ion are different in the two scenarios Diss2 and Diss4 (left and middle pictures), the dissolution patterns are almost the same, and so hydrogen ion concentration (pH) of the injected water is the primary parameter controlling dissolution in the porous medium. In contrast, little dolomite has been dissolved in scenario Diss5 (Fig. 12, right picture), because the hydrogen ion concentration is 10 times smaller and hence the water is less acidic than Diss2 and Diss4.

For the precipitation scenario (Prec1), the concentration distributions of different chemical species after 10 days of

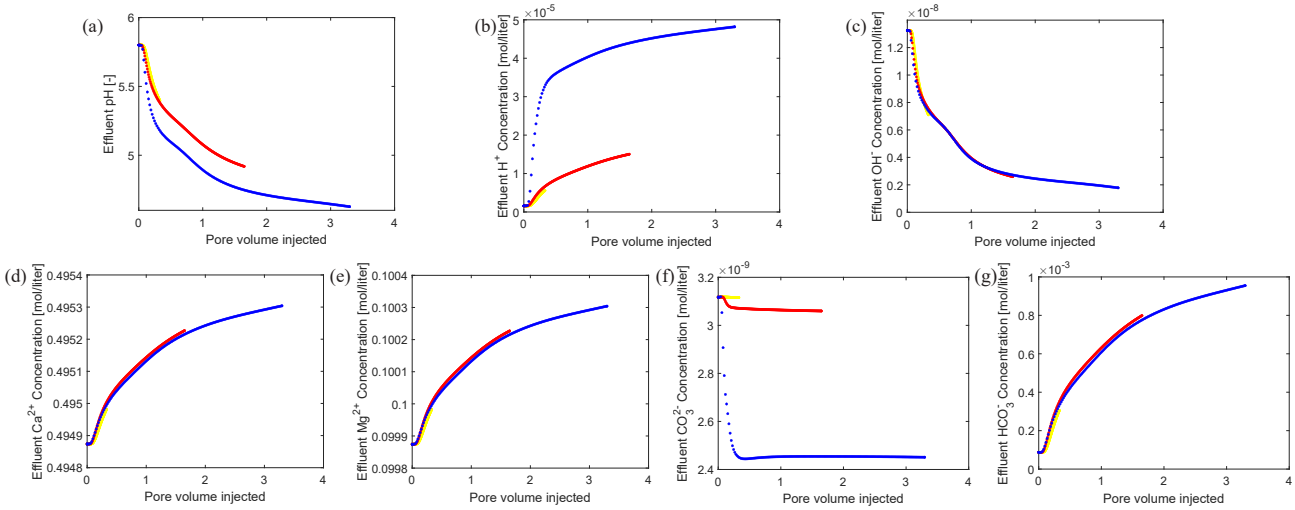

Fig. 9. Effluent concentrations of aqueous species over pore volume injected for Diss1 (yellow), Diss2 (red) and Diss3 (blue). (a) pH, (b) H^+, (c) OH^-, (d) Ca^{2+}, (e) Mg^{2+}, (f) $CO_3{}^{2-}$ and (g) $HCO_3{}^-$.

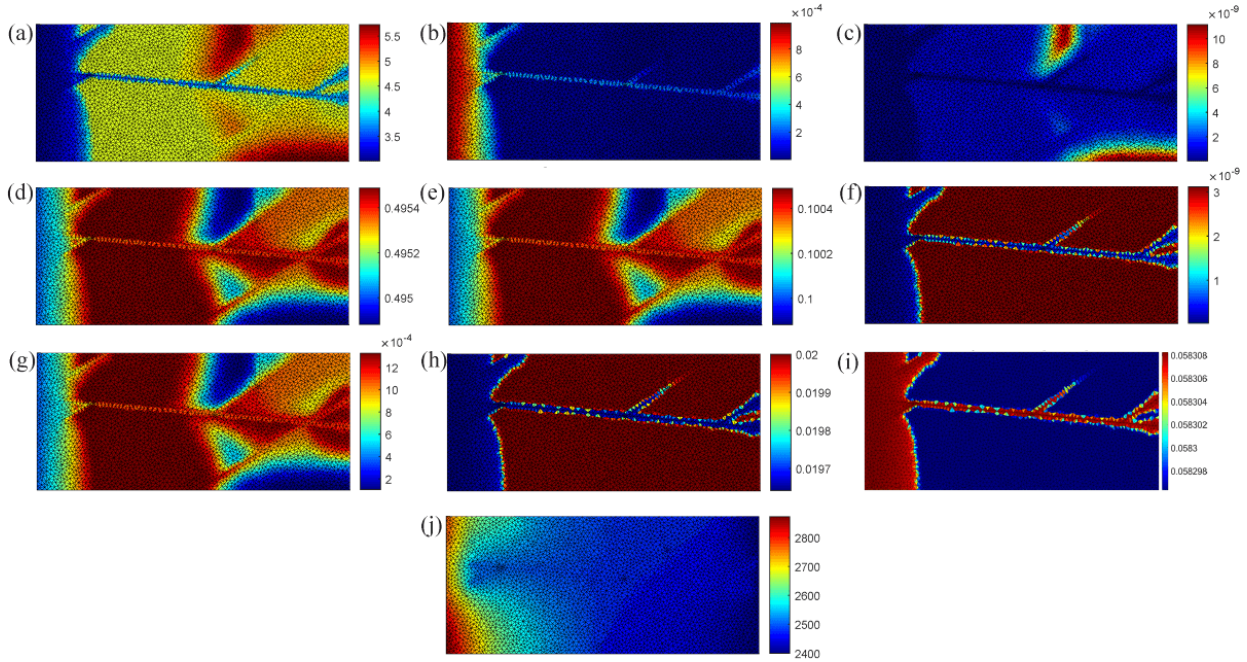

Fig. 10. Distribution of aqueous and mineral species concentrations [mol/liter], porosity [-], and pressure [Psia] for Diss3 after 50 days of injection. Distribution of (a) pH, (b) H^+, (c) OH^-, (d) Ca^{2+}, (e) Mg^{2+}, (f) $CO_3{}^{2-}$, (g) $HCO_3{}^-$, (h) $CaMg(CO_3)_2$, (i) porosity and (j) pressure.

injection are depicted in Fig. 13. In this scenario, the injected water is a bit less acidic than the formation water ($10^{-6} < 10^{-5.8}$). As the water is injected into the caprock, hydrogen ion concentration decreases, due to the higher basicity of the injected water. However, near the outlet, hydrogen ion concentration has increased because of dolomite precipitation. The injected water has also led to decrease in calcium and magnesium concentration in the porous medium, which is due to precipitation and also their lower concentrations in the injected water. In this scenario, precipitation mostly occurs in the vicinity of the fractures, particularly at the tip of the fractures near the outlet.

6.3 Comparison of DFM and EDFM models

Scenario Diss1 is also simulated using the EDFM model, and the results are shown in Fig. 14. Comparing the aqueous and mineral concentration distribution patterns of the DFM and EDFM models demonstrate that the two models give the same results. Plotting the total dolomite mole over time for the two models also confirms very close similarity in the results (Fig. 15). This is very encouraging as gridding for EDFM is substantially easier than for DFM. In the EDFM approach, the fractures do not need to match edges/faces of the computational grid and the meshing of the fractures is completely independent from the matrix (Lie and Møyner, 2021). This

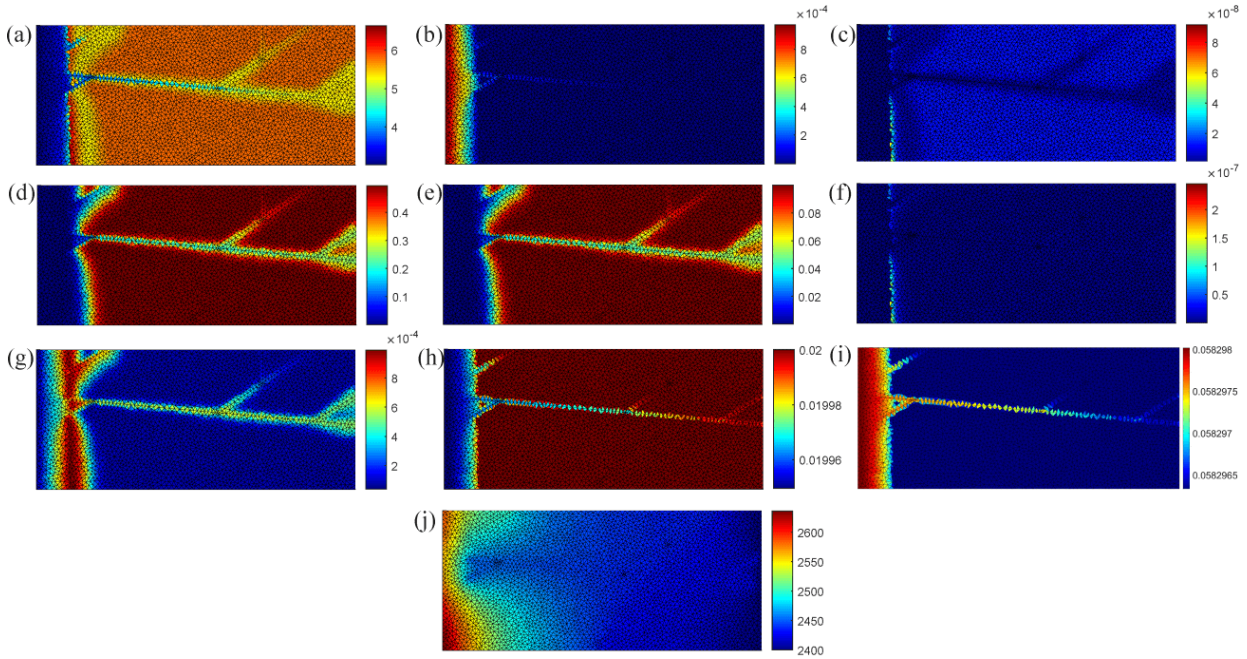

Fig. 11. Distribution of aqueous and mineral species concentrations [mol/liter], porosity [-], and pressure [Psia] for Diss4 after 7 days of injection. Distribution of (a) pH, (b) H^+, (c) OH^-, (d) Ca^{2+}, (e) Mg^{2+}, (f) $CO_3{}^{2-}$, (g) $HCO_3{}^-$, (h) $CaMg(CO_3)_2$, (i) porosity and (j) pressure.

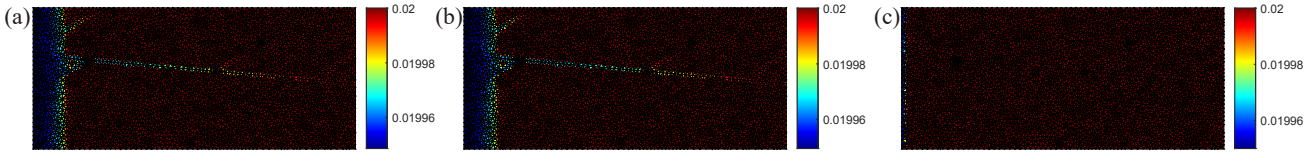

Fig. 12. Dolomite concentration [mol/liter] patterns for (a) Diss2, (b) Diss4 and (c) Diss5 after 7 days of injection.

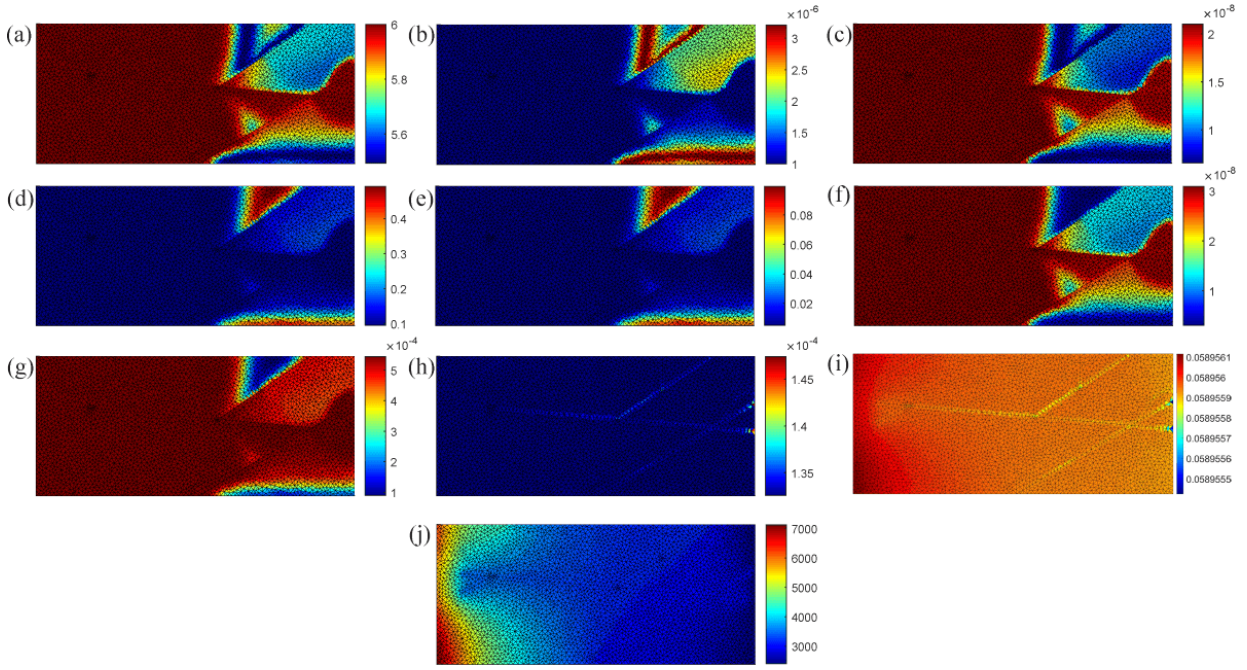

Fig. 13. Distribution of aqueous and mineral species concentrations [mol/liter], porosity [-], and pressure [Psia] for Prec1 after 10 days of injection. Distribution of (a) pH, (b) H^+, (c) OH^-, (d) Ca^{2+}, (e) Mg^{2+}, (f) $CO_3{}^{2-}$, (g) $HCO_3{}^-$, (h) $CaMg(CO_3)_2$, (i) porosity and (j) pressure.

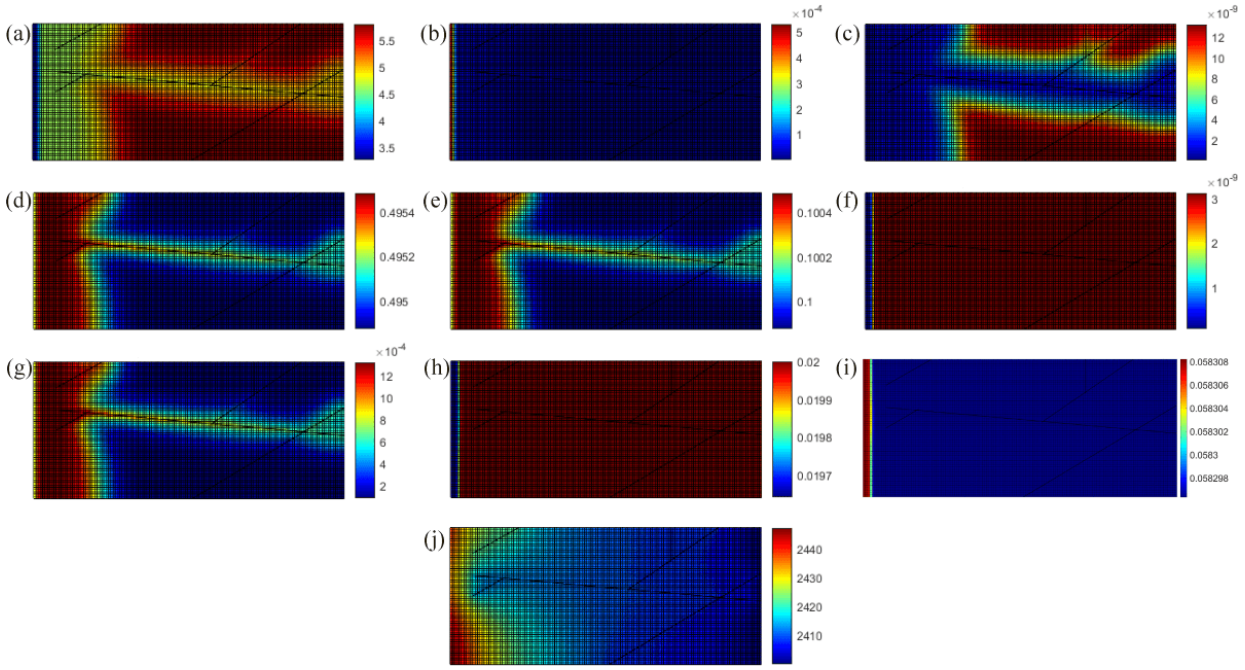

Fig. 14. Distribution of mineral and aqueous species concentrations [mol/liter], porosity [-], and pressure [Psia] in Diss1 after 50 days of injection using the EDFM model. Distribution of (a) pH, (b) H^+, (c) OH^-, (d) Ca^{2+}, (e) Mg^{2+}, (f) $CO_3{}^{2-}$, (g) $HCO_3{}^-$, (h) $CaMg(CO_3)_2$, (i) porosity and (j) pressure.

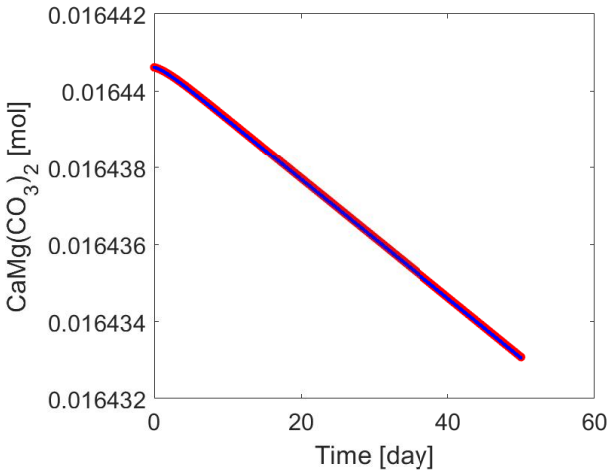

Fig. 15. Total dolomite mole change over time for Diss 1. Red markers: DFM and blue markers: EDFM.

enables the utilization of Cartesian grid, which leads to a reduction in the run time of the EDFM model because by using the aforementioned grid, the EDFM model requires fewer grid cells than the DFM model. As a result, the run time of the EDFM model is shorter than that of the DFM model. As an example, for Diss1, the run time of DFM model is about 155 minutes, while that of EDFM is about 135 minutes. In contrast, The EDFM model has a disadvantage. This model is only suitable for conductive fractures, i.e., it produces significant errors when fractures are sealed and form barriers to flow (Lie and Møyner, 2021). This disadvantage is not tested in this study.

7. Conclusions

In this study, a species-based reactive transport module in MRST is presented that is compatible with both DFM and EDFM modules of MRST. The module uses the SFI approach to solve the system of non-linear equations of the isothermal reactive transport problem considered in the study. The developed module has been validated against the commercial simulator GEM-GHG of CMG and realized that the solver must be iterative in order to achieve enough accuracy. It was also concluded that the solver is not suitable for scenarios in which the concentrations of mineral and fluid species change rapidly, otherwise the solver may face convergence issues. The module was illustrated by investigating the impact of acidic brine on the dissolution of a fractured dolomitic porous medium. The simulations demonstrate that as the hydrogen ion concentration in the injected water is higher, dissolution occurs more extensively, but changes in concentrations of the other aqueous species did not show much influence on dolomite mass. It was also shown that at higher flow rates, dissolution substantially affects permeability throughout the domain, while at smaller flow rates, dissolution only occurs in the vicinity of the inlet during the simulation time. Therefore, higher injection rate and hydrogen ion concentration could increase the likelihood of breaching a confining unit, but the concentrations of the aqueous species except the hydrogen ion are not as effective on the sealing capacity of the caprock considered in this model. Comparing the results of the DFM and EDFM models demonstrated that the two models give the same results in terms of aqueous and mineral concentration patterns and total dolomite mole in the system even though the EDFM model can be discretized more easily and also results

in a shorter run time.

Acknowledgements

Part of this work was funded by the European Union's Horizon 2020 research and innovation programs SECURe under grant agreement number 764531.

Conflict of interest

The authors declare no competing interest.

References

Abd, A. S., Abushaikha, A. S. Reactive transport in porous media: A review of recent mathematical efforts in modeling geochemical reactions in petroleum subsurface reservoirs. SN Applied Sciences, 2021, 3: 401.

Ahusborde, E., El Ossmani, M. A sequential approach for numerical simulation of two-phase multicomponent flow with reactive transport in porous media. Mathematics and Computers in Simulation, 2017, 137: 71-89.

Ahusborde, E., El Ossmani, M., Moulay, M. I. A fully implicit finite volume scheme for single phase flow with reactive transport in porous media. Mathematics and Computers in Simulation, 2019, 164: 3-23.

Ahusborde, E., Kern, M., Vostrikov, V. Numerical simulation of two-phase multicomponent flow with reactive transport in porous media: Application to geological sequestration of CO_2. ESAIM: Proceedings and Surveys, 2015, 50: 21-39.

Andrews, E., Hyman, J., Sweeney, M., et al. Fracture intensity impacts on reaction front propagation and mineral weathering in three-dimensional fractured media. Water Resources Research, 2023, 59(2): e2022WR032121.

Applegate, D., Appleyard, P. Capability for hydrogeochemical modelling within discrete fracture networks. Energies, 2022, 15: 6199.

Banshoya, S. I., Berre, I., Keilegavlen, E. Simulation of reactive transport in fractured porous media. Transport in Porous Media, 2023, 2: 643-667.

Barnes, D. A., Bacon, D. H., Kelley, S. R. Geological sequestration of carbon dioxide in the cambrian mount simon sandstone: Regional storage capacity, site characterization, and large-scale injection feasibility, michigan basin. Environmental Geosciences, 2009, 16: 163-183.

Bear, J. Dynamics of Fluids in Porous Media. New York, USA, Dover Publications, 2013.

Berre, I., Doster, F., Keilegavlen, E. Flow in fractured porous media: A review of conceptual models and discretization approaches. Transport in Porous Media, 2019, 130: 215-236.

Billings, M. P. Structural Geology. New Jersey, USA, Prentice-Hall, 1972.

Cao, H. Development of techniques for general purpose simulators. Stanford, Stanford University, 2002.

Chen, Y., Ma, G., Wang, H. The simulation of thermo-hydro-chemical coupled heat extraction process in fractured geothermal reservoir. Applied Thermal Engineering, 2018, 143: 859-870.

Colin, M., Xavier, R., Halvor, N., et al. Robust chemical solver for fully-implicit simulations. ArXiv Preprint ArXiv:1806.03010, 2018.

de Hoop, S., Jones, E., Voskov, D. Accurate geothermal and chemical dissolution simulation using adaptive mesh refinement on generic unstructured grids. Advances in Water Resources, 2021, 154: 103977.

de Hoop, S., Voskov, D., Bertotti, G. Studying the effects of heterogeneity on dissolution processes using operator based linearization and high-resolution lidar data. Paper Presented at ECMOR XVII, Edinburgh, United Kingdom, 14-17 September, 2020.

Deng, H., Fitts, J. P., Crandall, D., et al. Alterations of fractures in carbonate rocks by CO_2-acidified brines. Environmental Science & Technology, 2015, 49: 10226-10234.

Elgendy, A., Pizzolato, A., Maniglio, M., et al. Reactive transport modelling of H_2 storage in depleted gas fields: An approach to implement biogeochemical reactions in a compositional reservoir simulator. Paper SPE 214434 Presented at the SPE EuropEC-Europe Energy Conference featured at the 84th EAGE Annual Conference & Exhibition, Vienna, Austria, 5-8 June, 2023.

Fahs, M., Carrayrou, J., Younes, A., et al. On the efficiency of the direct substitution approach for reactive transport problems in porous media. Water, Air, and Soil Pollution, 2008, 193: 299-308.

Fan, Y., Durlofsky, L. J., Tchelepi, H. A. Numerical simulation of the *in-situ* upgrading of oil shale. SPE Journal, 2010, 15: 368-381.

Fan, Y., Durlofsky, L. J., Tchelepi, H. A. A fully-coupled flow-reactive-transport formulation based on element conservation, with application to CO_2 storage simulations. Advances in Water Resources, 2012, 42: 47-61.

Fang, Y., Yeh, G. T., Burgos, W. D. A general paradigm to model reaction-based biogeochemical processes in batch systems. Water Resources Research, 2003, 39(4): 1083.

Fitts, J. P., Peters, C. A. Caprock fracture dissolution and CO_2 leakage. Reviews in Mineralogy and Geochemistry, 2013, 77: 459-479.

Franc, J., Møyner, O., Tchelepi, H. A. Coupling-strength criteria for sequential implicit formulations. Journal of Computational Physics, 2023, 492: 112413.

Gholami, R. Hydrogen storage in geological porous media: Solubility, mineral trapping, H_2S generation and salt precipitation. Journal of Energy Storage, 2023, 59: 106576.

Gilmore, T., Bonneville, A., Sullivan, C., et al. Characterization and design of the FutureGen 2.0 carbon storage site. International Journal of Greenhouse Gas Control, 2016, 53: 1-10.

Gong, B., Zhang, Y., Fan, Y., et al. A novel approach to model enhanced coal bed methane recovery with discrete fracture characterizations in a geochemical simulator. Journal of Petroleum Science and Engineering, 2014,

124: 198-208.

Gylling, B., Trinchero, P., Molinero, J., et al. A DFN-based high performance computing approach to the simulation of radionuclide transport in mineralogically heterogeneous fractured rocks. Paper H51C-1479 Presented at the AGU Fall Meeting Abstracts, San Francisco, California, 12-16 December, 2016.

Hammond, G., Lichtner, P., Lu, C. Subsurface multiphase flow and multicomponent reactive transport modeling using high-performance computing. Journal of Physics: Conference Series, 2007, 78(1): 012025.

Hammond, G. E., Valocchi, A. J., Lichtner, P. C. Application of Jacobian-free Newton-Krylov with physics-based preconditioning to biogeochemical transport. Advances in Water Resources, 2005, 28: 359-376.

Hemme, C., Van Berk, W. Hydrogeochemical modeling to identify potential risks of underground hydrogen storage in depleted gas fields. Applied Sciences, 2018, 8: 2282.

Hu, M., Rutqvist, J. Multi-scale coupled processes modeling of fractures as porous, interfacial and granular systems from rock images with the numerical manifold method. Rock Mechanics and Rock Engineering, 2022, 55: 3041-3059.

Jiang, C., Wang, X., Pu, S., et al. Incipient karst generation in jointed layered carbonates: Insights from three-dimensional hydro-chemical simulations. Journal of Hydrology, 2022, 610: 127831.

Jiang, C., Wang, X., Pu, S., et al. Karst genesis and wormhole formation in carbonate joint networks: A comparison between 3D and 2D modeling. Journal of Hydrology, 2023, 619: 129303.

Jiang, Y. Techniques for modeling complex reservoirs and advanced wells. Stanford, Stanford University, 2007.

Kampman, N., Bertier, P., Busch, A., et al. Validating reactive transport models of CO2-brine-rock reactions in caprocks using observations from a natural CO_2 reservoir. Energy Procedia, 2017, 114: 4902-4916.

Karimi-Fard, M., Durlofsky, L. J., Aziz, K. An efficient discrete-fracture model applicable for general-purpose reservoir simulators. SPE Journal, 2004, 9: 227-236.

Keller, S. J. Analyses of subsurface brines of Indiana. Bloomington, Indiana, US Geological & Water Survey, 1983.

Krogstad, S., Lie, K. A., Møyner, O., et al. MRST-AD-an open-source framework for rapid prototyping and evaluation of reservoir simulation problems. Paper SPE 173317 Presented at SPE Reservoir Simulation Conference, Houston Texas, 23-25 February, 2015.

Labotka, D. M., Panno, S. V., Locke, R. A., et al. Isotopic and geochemical characterization of fossil brines of the Cambrian Mt. Simon sandstone and Ironton-Galesville formation from the Illinois Basin, USA. Geochimica et Cosmochimica Acta, 2015, 165: 342-360.

Lasaga, A. C. Chemical kinetics of water-rock interactions. Journal of Geophysical Research: Solid Earth, 1984, 89: 4009-4025.

Lee, K. J., Moridis, G. J., Ehlig-Economides, C. A. Compositional simulation of hydrocarbon recovery from oil shale reservoirs with diverse initial saturations of fluid phases by various thermal processes. Energy Exploration & Exploitation, 2017, 35: 172-193.

Li, J., Tomin, P., Tchelepi, H. Sequential fully implicit newton method for flow and transport with natural black-oil formulation. Computational Geosciences, 2023, 27: 485-498.

Li, S., Kang, Z., Feng, X., et al. Three-dimensional hydrochemical model for dissolutional growth of fractures in karst aquifers. Water Resources Research, 2020, 56: e2019WR025631.

Lie, K. A. An Introduction to Reservoir Simulation Using MATLAB/GNU Octave: User Guide for the MATLAB Reservoir Simulation Toolbox (MRST). Cambridge, UK, Cambridge University Press, 2019.

Lie, K. A., Moyner, O. Advanced Modelling with the MATLAB Reservoir Simulation Toolbox. Cambridge, UK, Cambridge University Press, 2021.

Liu, P., Yao, J., Couples, G. D., et al. Numerical modelling and analysis of reactive flow and wormhole formation in fractured carbonate rocks. Chemical Engineering Science, 2017, 172: 143-157.

Liu, X., Ormond, A., Bartko, K., et al. A geochemical reaction-transport simulator for matrix acidizing analysis and design. Journal of Petroleum Science and Engineering, 1997, 17: 181-196.

Luhmann, A. J., Kong, X., Tutolo, B. M., et al. Experimental dissolution of dolomite by CO_2-charged brine at 100 °C and 150 bar: Evolution of porosity, permeability, and reactive surface area. Chemical Geology, 2014, 380: 145-160.

Machado, M. V. B., Delshad, M., Sepehrnoori, K. Modeling self-sealing sechanisms in fractured carbonates induced by CO_2 injection in saline aquifers. ACS Omega, 2023, 8: 48925.

Mayer, K. U., Frind, E. O., Blowes, D. W. Multicomponent reactive transport modeling in variably saturated porous media using a generalized formulation for kinetically controlled reactions. Water Resources Research, 2002, 38: 13-1-13-21.

Mehnert, E., Damico, J. R., Grigsby, N. P., et al. Geologic carbon sequestration in the Illinois basin: Numerical modeling to evaluate potential impacts. Champaign, Illinois, Illinois State Geological Survey, 2019.

Moinfar, A., Varavei, A., Sepehrnoori, K., et al. Development of an efficient embedded discrete fracture model for 3D compositional reservoir simulation in fractured reservoirs. SPE Journal, 2014, 19: 289-303.

Molson, J., Aubertin, M., Bussière, B. Reactive transport modelling of acid mine drainage within discretely fractured porous media: Plume evolution from a surface source zone. Environmental Modelling & Software, 2012, 38: 259-270.

Morel, F. M., Hering, J. G. Principles and Applications of Aquatic Chemistry. New York, USA, John Wiley & Sons, 1993.

Nghiem, L., Sammon, P., Grabenstetter, J., et al. Modeling CO_2 storage in aquifers with a fully-coupled geochemical EOS compositional simulator. Paper SPE 89474 Pre-

sented at SPE Improved Oil Recovery Conference, Tulsa, Oklahoma, 17-21 April, 2004.

Nghiemw, L., Shrivastavar, A., Kohse, B., et al. Simulation of CO_2 EOR and sequestration processes with a geochemical EOS compositional simulator. Paper PETSOC-2004-051 Presented at Canadian International Petroleum Conference, Calgary, Alberta, 8-10 June, 2004.

Palandri, J. L., Kharaka, Y. K. A compilation of rate parameters of water-mineral interaction kinetics for application to geochemical modeling. Reston, Viriginia, US Geological Survey, 2004.

Palkovic, M. J. Depositional characterization of the Eau Claire formation at the Illinois Basin-Decatur Project: Facies, mineralogy and geochemistry. Urbana, Illinois, University of Illinois at Urbana-Champaign, 2015.

Parkhurst, D. L., Appelo, C. User's guide to PHREEQC (Version 2): A computer program for speciation, batch-reaction, one-dimensional transport, and inverse geochemical calculations. Denver, Colorado, US Geological Survey, 1999.

Pruess, K. TOUGH2-A general-purpose numerical simulator for multiphase fluid and heat flow. Berkeley, California, Lawrence Berkeley Laboratory, 1991.

Pruess, K., Garcia, J., Kovscek, T., et al. Intercomparison of numerical simulation codes for geologic disposal of CO_2. Berkeley, California, Lawrence Berkeley National Laboratory, 2002.

Saaltink, M. W., Carrera, J., Ayora, C. On the behavior of approaches to simulate reactive transport. Journal of Contaminant Hydrology, 2001, 48: 213-235.

Salih, H. H., Dastgheib, S. A. Treatment of a hypersaline brine, extracted from a potential CO_2 sequestration site, and an industrial wastewater by membrane distillation and forward osmosis. Chemical Engineering Journal, 2017, 325: 415-423.

Seigneur, N., Socié, A., Mayer, K. U. A compositional global implicit approach for modeling coupled multicomponent reactive transport. Water Resources Research, 2023, 59: e2021WR031774.

Shaik, R., Tomin, P., Voskov, D. Modeling of near-well matrix acidization. Paper Presented at 43rd Workshop on Geothermal Reservoir Engineering, Stanford University, Stanford, California, 12-14 February, 2018.

Sherman, T., Sole-Mari, G., Hyman, J., et al. Characterizing reactive transport behavior in a three-dimensional discrete fracture network. Transport in Porous Media, 2023, 146: 307-327.

Shewchuk, J. R. Triangle: Engineering a 2D auality mesh generator and Delaunay triangulator, Workshop on applied computational geometry, Paper Presented at Applied Computational Geometry Towards Geometric Engineering, Philadelphia, PA, 27-28 May, 1996.

Song, G., Song, X., Ji, J., et al. Evolution of fracture aperture and thermal productivity influenced by chemical reaction in enhanced geothermal system. Renewable Energy, 2022a, 186: 126-142.

Song, G., Song, X., Xu, F., et al. Numerical parametric investigation of thermal extraction from the enhanced geothermal system based on the thermal-hydraulic-chemical coupling model. Journal of Cleaner Production, 2022b, 352: 131609.

Steefel, C. I., Hu, M. Reactive transport modeling of mineral precipitation and carbon trapping in discrete fracture networks. Water Resources Research, 2022, 58: e2022WR032321.

Steefel, C. I., Lasaga, A. C. A coupled model for transport of multiple chemical species and kinetic precipitation/dissolution reactions with application to reactive flow in single phase hydrothermal systems. American Journal of science, 1994, 294: 529-592.

Stein, E., Frederick, J. M., Hammond, G. E., et al. Modeling Coupled Reactive Flow Processes in Fractured Crystalline Rock. Albuquerque, New Mexico, Sandia National Laboratory, 2017.

Thibeau, S., Nghiem, L. X., Ohkuma, H. A modeling study of the role of selected minerals in enhancing CO_2 mineralization during CO_2 aquifer storage. Paper SPE 109739 Presented at SPE Annual Technical Conference and Exhibition Anaheim, California, 11-14 November, 2007.

Vu, P. T., Ni, C., Li, W., et al. Particle-based workflow for modeling uncertainty of reactive transport in 3D discrete fracture networks. Water, 2019a, 11(12): 2502.

Vu, P. T., Ni, C., Li, W., et al. Particle tracking approach to model chemical reaction transport in 3D discrete fracture networks. Geophysical Research Abstracts, 2019b, 21: EGU2019-6678.

Wang, T., Sun, Z., Sun, H., et al. Development of a scalable parallel compositional simulator for thermo-hydromechanical coupling in fractured rocks using an embedded discrete fracture model. SPE Journal, 2024, 29(5): 2545-2565.

Xu, T., Pruess, K. Modeling multiphase non-isothermal fluid flow and reactive geochemical transport in variably saturated fractured rocks: 1. methodology. American Journal of science, 2001, 301: 16-33.

Xu, T., Sonnenthal, E., Spycher, N., et al. TOUGHREACT user's guide: A simulation program for non-isothermal multiphase reactive geochemical transport in variable saturated geologic media. Berkeley, USA, Lawrence Berkeley National Laboratory, 2004.

Yan, B., Mi, L., Wang, Y., et al. Multi-porosity multi-physics compositional simulation for gas storage and transport in highly heterogeneous shales. Journal of Petroleum Science and Engineering, 2018, 160: 498-509.

Yeh, G., Tripathi, V. A critical evaluation of recent developments in hydrogeochemical transport models of reactive multichemical components. Water Resources Research, 1989, 25: 93-108.

Zhang, W., Han, D., Wang, B., et al. Thermal-hydraulic-mechanical-chemical modeling and simulation of an enhanced geothermal system based on the framework of extended finite element methods-embedded discrete fracture model. Journal of Cleaner Production, 2023, 415: 137630.